# Raman scattering by LO-phonon–plasmon coupled modes in $Ga_{1-x}In_xAs_ySb_{1-y}$: Role of Landau damping

Ramon Cuscó, Esther Alarcón-Lladó, and Luis Artús
*Institut Jaume Almera, Consell Superior d'Investigacions Científiques (CSIC), Lluís Solé i Sabarís s.n., 08028 Barcelona, Spain*

Wilbur S. Hurst and James E. Maslar
*Chemical Science and Technology Laboratory, National Institute of Standards and Technology, 100 Bureau Drive, Stop 8360, Gaithersburg, Maryland 20899-8360, USA*

(Received 15 March 2010; revised manuscript received 27 April 2010; published 20 May 2010)

We present a detailed investigation of the phonons and longitudinal-optical-phonon–plasmon coupled modes in the $Ga_{1-x}In_xAs_ySb_{1-y}$ alloy by means of Raman scattering. A generalization of the dielectric Raman line-shape model to quaternary alloys is described and used to analyze the Raman spectra of a set of *n*-type $Ga_{1-x}In_xAs_ySb_{1-y}$ layers with $x=0.15$, $y=0.13$, and electron densities ranging from $2.8\times10^{17}$ to $3.7\times10^{18}$ $cm^{-3}$. Landau-damping effects are found to be essential to correctly describe the coupled modes that occur in the phonon-frequency range. Differences in the electron-density dependence of these modes between 80 K and room temperature are observed and attributed to different Landau-damping regimes. The plasmonlike $L^+$ mode is observed to shift to lower frequencies when the temperature is increased from 80 K to room temperature. This frequency shift is explained in terms of thermal population of the *L* valleys.

DOI: 10.1103/PhysRevB.81.195212 PACS number(s): 78.30.Fs, 63.20.−e

## I. INTRODUCTION

III-V mixed crystals are of interest not only in the study of fundamental aspects of lattice dynamics in disordered systems but also for their wide range of applications in band-gap engineering. Quaternary alloys offer higher flexibility for tuning the band gap while maintaining the lattice match with the substrate. The quaternary alloy $Ga_{1-x}In_xAs_ySb_{1-y}$ lattice matched to GaSb is a direct narrow-band-gap semiconductor which allows the band gap to be reduced close to 0.5 eV (Ref. 1) and finds important applications in high-performance thermophotovoltaic devices. The GaInAsSb/GaSb system has produced the highest performance thermophotovoltaic devices to date.[2] Other applications of this alloy include infrared lasers and photodetectors operating at wavelengths beyond 2 $\mu$m.[3–5] In spite of the technological interest of $Ga_{1-x}In_xAs_ySb_{1-y}$, the growth of these alloys is difficult due to a large miscibility gap[6] and fundamental studies of their optical properties are scarce. Early studies of the lattice dynamics of $Ga_{1-x}In_xAs_ySb_{1-y}$ using Raman scattering were carried out for various compositions lattice matched to GaSb, InAs, and InP.[7] These studies suggested a three-mode behavior for the quaternary alloy, although the Raman spectra of those early samples were rather poor and the InSb-like mode was not observed in most of the samples studied. Other Raman-scattering characterizations of $Ga_{1-x}In_xAs_ySb_{1-y}$/InAs epilayers[8] have been analyzed following Ref. 7 but they are generally limited by the weak signal of the Raman spectra. More recently, Raman scattering was used to characterize Te doped $Ga_{1-x}In_xAs_ySb_{1-y}$/GaSb layers.[9] Further work is needed to establish a more detailed picture of the long-wavelength lattice dynamics in the $Ga_{1-x}In_xAs_ySb_{1-y}$ alloy over a broader composition range. The optical constants of $Ga_{1-x}In_xAs_ySb_{1-y}$/GaSb epilayers with the same composition as those studied in the present work were determined by spectral ellipsometry.[10]

Raman scattering can also be utilized to probe effectively in a contactless way the free-charge density in doped polar semiconductors by analyzing the longitudinal-optical (LO)-phonon–plasmon coupled modes (LOPCMs).[11] In general, two branches of the coupled modes labeled $L^+$ and $L^-$ are observed in high-mobility *n*-type binary semiconductors. In degenerate material, the $L^+$ has a plasmonlike character and its frequency depends strongly on free-charge density. LOPCMs have been extensively studied in many *n*-type doped III-V binary semiconductors[11] and carrier-concentration values derived from their Raman line-shape analysis have been shown to be in good agreement with Hall-effect measurements.[12–14] Despite their fundamental interest, much less studies have been directed to LOPCMs in III-V alloy semiconductors.[15–17] Recently, the high sensitivity to free-electron concentration of the $L^+$ coupled mode has been employed to perform a Raman spectroscopic determination of electron concentration in *n*-type GaInAsSb.[18] The existence of separate LO branches associated with the different anion-cation bondings in alloys leads to the observation of additional coupled modes whose character differs from those of the typical $L^+$ and $L^-$ modes of binary semiconductors. The *n*-type $Al_xGa_{1-x}As$ alloy exemplifies the typical coupled-mode behavior that is expected in ternary alloys.[15] Besides the usual $L^+$ and $L^-$ modes, an additional coupled mode $L_0$ was observed in the frequency gap between the two sets of zone-center optical modes. The frequency of this mode increases with free-electron density and displays phononlike character at both high- and low-carrier densities. The coupled-mode behavior in the two-mode $Al_xGa_{1-x}As$ alloy could be well understood from the straightforward analysis of the zeros of the dielectric function.[15] However, this simple picture cannot be generalized to all alloys. In fact, a different coupled-mode behavior was reported in $In_xGa_{1-x}As$,[16,17] where only the $L^+$ mode shows a frequency increase with electron density whereas the remaining coupled modes decrease in frequency as the electron density

 

increases. This behavior was ascribed to the specificity of material properties such as low electron effective mass and low phonon energies which result in heavy Landau damping of the lower energy coupled modes.[17]

For low In and As compositions, the quaternary alloy $Ga_{1-x}In_xAs_ySb_{1-y}$ also exhibits low values of electron effective-mass and optical-phonon frequencies. Four different types of oscillators are in principle expected to couple with the plasma excitations. In this work we present a Raman-scattering study of LOPCMs in GaInAsSb and we discuss the results in the light of the line-shape models most usually employed to describe coupled modes in semiconductors. Specific characteristics of the alloy conduction bands such as its marked nonparabolicity at the Γ point and the presence of secondary minima at *L* are duly taken into account. We show that the behavior of the lower frequency coupled modes is not accounted for by the simple Drude or hydrodynamical (HD) models and only the Lindhard-Mermin (LM) model,[19] which includes Landau-damping effects, can explain the observed carrier-density dependence of the lower frequency coupled modes.

The paper is organized as follows. In Sec. II we describe the set of GaInAsSb layers used in this study and the experimental conditions for the Raman-scattering measurements. Section III presents a generalization of the dielectric Raman line-shape model to quaternary alloys and a discussion of the different approaches to model the free-electron contribution to the susceptibility. The lattice dynamics and Raman spectra of the undoped GaInAsSb alloy are discussed in Sec. IV A. The LOPCM behavior predicted by the various line-shape models is analyzed in Sec. IV B. Finally, in Sec. IV C we present and analyze the Raman spectra of *n*-type GaInAsSb samples obtained at room temperature and at 80 K. Our results are compared with the theoretical predictions of the LM model.

## II. EXPERIMENT

Five *n*-type doped $Ga_{0.85}In_{0.15}As_{0.13}Sb_{0.87}$ epitaxial layers were studied. The layers were grown by organometallic vapor-phase epitaxy on semi-insulating GaAs (001) substrates in a vertical flow, rotating-disk reactor. The samples were doped with Te using diethyltellurium following the growth technique described elsewhere.[20,21] The In and Al contents of the epilayers were determined from double-crystal x-ray diffraction measurements. Electron concentration and mobility of the GaInAsSb epilayers were determined using single magnetic field Hall-effect measurements based on the van der Pauw method. Ohmic contacts were made to GaInAsSb using indium metal. Measurements were performed at 77 K using a 1 T magnetic field. At this temperature, the correction to the effective electron density probed by the Hall measurements due to *L*-minima conduction[18,22] is totally negligible for all the samples but the one with the highest electron density, where it amounts to about 2%. The electron concentrations derived from the Hall measurements on these samples, labeled A to E, were, respectively, $2.8\times10^{17}$, $4.8\times10^{17}$, $9.7\times10^{17}$, $2.1\times10^{18}$, and $3.7\times10^{18}$ $cm^{-3}$. A nominally undoped reference sample with the same composition was also grown.

Raman-scattering measurements were performed at room temperature and at 80 K in $z(x,y)\bar{z}$ backscattering configuration, where *x*, *y*, and *z* are parallel to the [100], [010], and [001] directions, respectively. The spectra were obtained using 780.0 nm excitation wavelength from a Ti:sapphire laser. The scattered light was analyzed using a Jobin-Yvon T64000 spectrometer equipped with a charge coupled device detector cooled with liquid nitrogen. The single stage configuration of the spectrometer was used to maximize the instrument throughput. In this configuration, for 100 $\mu$m slit width the spectrometer bandwidth is $\approx 0.8$ $cm^{-1}$.

## III. THEORY

### A. Line-shape model

In polar semiconductors the collective oscillations of the free-electron gas couple with the longitudinal-optical modes via their macroscopic fields. The fluctuation-dissipation formalism developed by Hon and Faust[23] conveniently describes such coupling and has been proven to provide an accurate modeling of LO-phonon–plasmon coupled modes in binary semiconductors[12] and ternary alloys.[17] The model, which is based on the linear response of the free-charge-lattice system to generalized strains taking into account electrostatic interaction between sublattice polarizations, can be readily extended to the $A_xB_{1-x}C_yD_{1-y}$ quaternary alloys by considering some simple assumptions on the dielectric properties of the alloy. Following the ideas of the cell isodisplacement theory,[24] we consider sublattice cells of four kinds: *AC*, *AD*, *BC*, and *BD* ($i=1$, 2, 3, and 4, respectively) and thus we express the complex dielectric function of the alloy as

$$\varepsilon(\omega;x,y)=\varepsilon_\infty(x,y)\left(1+\sum_{i=1}^{4}\frac{\Omega_{Pi}^2}{\omega_{\mathrm{TO},i}^2-\omega^2-i\omega\Gamma_I}\right), \quad (1)$$

where $\omega_{\mathrm{TO},i}$ and $\Omega_{P,i}$ are, respectively, the transverse-optical frequency and the ionic plasma frequency of the *i*th sublattice. Assuming that the effective charges are weakly dependent on composition, the ionic plasma frequency is given by

$$\Omega_{Pi}^2=W_i\frac{\varepsilon_{\infty i}}{\varepsilon_\infty(x,y)}\Omega_{P,i}^{0\,2}. \quad (2)$$

Here, $\Omega_{P,i}^{0\,2}=\omega_{\mathrm{LO},i}^{0\,2}-\omega_{\mathrm{TO},i}^{0\,2}$ is the ionic plasma frequency squared for the *pure binaries* and $W_i$ is the statistical weight of the *i*th bond,

$$W_i=\begin{cases} xy & (i=1),\\ x(1-y) & (i=2),\\ (1-x)y & (i=3),\\ (1-x)(1-y) & (i=4). \end{cases} \quad (3)$$

Similarly, we also assume a linear dependence on composition for the Faust-Henry coefficients, $C_i=W_iC_i^0$, and for the high-frequency dielectric constant, $\varepsilon_\infty(x,y)=\Sigma_iW_i\varepsilon_{\infty,i}$, with $C_i^0$ and $\varepsilon_{\infty,i}$ the values corresponding to the pure binaries.

From the generalization of the Hon-Faust dielectric model[23] to a quaternary alloy whose dielectric response is described by Eq. (1), the differential Raman-scattering cross

section for deformation-potential and electro-optic mechanisms can be expressed as

$$\frac{\partial^2\sigma}{\partial\Omega\,\partial\,\omega} \propto [n(\omega)+1]\Im\left\{-\frac{1}{\varepsilon(\omega)}\left\{\frac{1}{4\pi}+2\sum_{i=1}^{4}\frac{\mathcal{A}_i}{\varepsilon_{\infty,i}}\chi_i + 4\pi\sum_{i\neq j=1}^{4}\left(\frac{\mathcal{A}_i\mathcal{A}_j}{\varepsilon_{\infty,i}\varepsilon_{\infty,j}}-\frac{\mathcal{A}_i^2}{\varepsilon_{\infty,i}^2}\right)\chi_i\chi_j-\left[1-\frac{4\pi\chi_e}{\varepsilon_\infty(x,y)}\right]\varepsilon_\infty(x,y)\sum_{i=1}^{4}\left(\frac{\mathcal{A}_i}{\varepsilon_{\infty,i}}\right)^2\chi_i\right\}\right\}. \quad (4)$$

Here, $\Im$ stands for the imaginary part and we have introduced

$$\mathcal{A}_i = C_i^0\frac{\omega_{\mathrm{TO},i}^2}{\Omega_{P,i}^{0\ 2}}, \quad (5)$$

the ionic sublattice susceptibilities

$$\chi_i = \frac{\varepsilon_{\infty,i}}{4\pi}W_i\frac{\Omega_{P,i}^{0\ 2}}{\omega_{\mathrm{TO},i}^2-\omega^2-i\omega\Gamma_I}, \quad (6)$$

and the electron plasma susceptibility $\chi_e$. For the evaluation of $\chi_e$ we use the Lindhard-Mermin prescription

$$\chi_e(q,\omega+i\Gamma_e) = \frac{(1+i\Gamma_e/\omega)\chi_e^L(q,\omega+i\Gamma_e)}{1+i\Gamma_e\chi_e^L(q,\omega+i\Gamma_e)/[\omega\chi_e^L(q,0)]}, \quad (7)$$

where $\chi_e^L(q,\omega)$ is the Lindhard susceptibility and $\Gamma_e$ is a phenomenological damping constant that takes into account collision-damping effects in the relaxation-time approximation. We calculate the electric susceptibility $\chi_e^L(q,\omega)$ by numerically evaluating the Lindhard integral

$$\chi_e^L(q,\omega) = \frac{e^2}{2\pi^3q^2}\int f(E_F,T,k)\frac{E(\mathbf{q}+\mathbf{k})-E(\mathbf{k})}{[E(\mathbf{q}+\mathbf{k})-E(\mathbf{k})]^2-(\hbar\omega)^2}d^3k, \quad (8)$$

where $f(E_F,T,k)$ is the Fermi distribution function for an electron gas with Fermi energy $E_F$ at temperature $T$ and $E(k)$ is the energy dispersion of the conduction band of the alloy. This model, which includes wave-vector dispersion, temperature, and nonparabolicity effects, has been shown to provide an accurate description of the electron plasma susceptibility in other III-V semiconductors.[11,12,17]

Simpler approaches to evaluating $\chi_e$ such as the Drude model[15,25] and the HD model[26–28] are often used in LOPCM studies. In the present work we compare the predictions of these models, which are basically classical models that neglect Landau-damping effects, with those of the LM model, where single-particle excitations (SPEs) between electronic states are taken into account. We consider the following Drude-type susceptibility:

$$\chi_e^D(\omega,q) = -\frac{\varepsilon_\infty}{4\pi}\frac{\omega_p^2(q)}{\omega(\omega+i\Gamma_e)}, \quad (9)$$

which can be obtained by expanding Eqs. (7) and (8) in powers of $q$ (small-$q$ limit). Wave-vector dispersion can be taken into account *ad hoc* in the Drude model by using a wave-vector-dependent plasma frequency[29]

$$\omega_p(q) = \omega_p\left\{1+\langle v^2\rangle\left[\frac{q}{\omega_p(q)}\right]^2\right\}^{1/2}, \quad (10)$$

where $\langle v^2\rangle$ is the electron mean-square velocity and $\omega_p$ is the plasma frequency of the electron gas. Alternatively, one can include a force term proportional to pressure gradients in the classical dynamical equations of the electron gas, which leads to the HD model susceptibility[26]

$$\chi_e^{\mathrm{HD}}(\omega,q) = -\frac{\varepsilon_\infty}{4\pi}\frac{\omega_p^2}{\omega^2-\langle v^2\rangle q^2+i\omega\Gamma_e}. \quad (11)$$

The $Ga_{1-x}In_xAs_ySb_{1-y}$ alloy is a direct narrow-band-gap semiconductor with a highly nonparabolic conduction band. In view of the lack of knowledge for this compound of physical parameters required to construct a higher order $\mathbf{k}\cdot\mathbf{p}$ model for the conduction band,[30] we use a simplified Kane's two-band model.[31,32] Ignoring spin-orbit interaction and considering the $m^*\ll m_e$ limit, the solution of Kane's secular determinant is given by

$$E(k) = \frac{1}{2}\left[\sqrt{E_0^2+4E_0\frac{\hbar^2k^2}{2m^*}}-E_0\right]. \quad (12)$$

At room temperature, a small but appreciable population of the $L$ conduction-band minima is expected. For simplicity, we assume isotropic $L$ minima with an average effective mass

$$\frac{1}{m_L^*} = \frac{1}{3}\left(\frac{2}{m_L^{t\,*}}+\frac{1}{m_L^{l\,*}}\right), \quad (13)$$

where $m_L^{t\,*}$ and $m_L^{l\,*}$ are, respectively, the transverse and longitudinal electron effective masses at $L$. We also consider the Maxwellian limit for the occupation of the $L$ minima,

$$N_L = 2\left(\frac{m_L^{\mathrm{DOS}}k_BT}{2\pi\hbar^2}\right)^{3/2}\exp\left(\frac{E_F-E_{\Gamma L}}{k_BT}\right). \quad (14)$$

Here $m_L^{\mathrm{DOS}}=4^{2/3}(m_L^{l\,*}m_L^{t\,*2})^{1/3}$ is the density-of-states effective mass at $L$ and $E_F$ is the Fermi energy. Then, if we neglect interband transitions,[11] the electrons at the $L$ minima yield an additive contribution to the electronic susceptibility[33,34]

$$\chi_L(\omega,q) = \frac{\varepsilon_\infty}{4\pi}\frac{1+\eta Z(\eta)}{(\lambda_Dq)^2}, \quad (15)$$

where $Z(\eta)$ is the classical plasma dispersion function, $\lambda_D$ is the Debye length, and $\eta$ is a dimensionless parameter defined as

$$\eta = \left(\frac{m_L^*}{2k_BT}\right)^{1/2}\frac{\omega}{q}. \quad (16)$$

The damping for the electrons in the $L$ valley was set according to a power-law-of-mass relation[35] as $\Gamma_L=\Gamma_e(m_L^*/m_\Gamma^*)^{3/2}$. The parameters used in the line-shape model are listed in Table I.

### B. Single-particle excitation regime

Coupled-mode excitations can be absorbed by conduction-band electrons provided that crystal momentum

TABLE I. Input parameters used for the LOPCM line-shape model. The indices $i$ stand for the $i$th binary compound, except for $\Gamma_I^i$ and $\omega_{\mathrm{TO},i}$, where they refer to the $i$th sublattice of the alloy.

| Symbol | Description | Value | | | | | Units |
|---|---|---|---|---|---|---|---|
| | | GaInAsSb | GaAs ($i=1$) | GaSb ($i=2$) | InAs ($i=3$) | InSb ($i=4$) | |
| $E_\Gamma$ [a] | Direct band-gap energy at $\Gamma$ | 0.542 | | | | | eV |
| $E_{\Gamma\text{-}L}$ [b] | $\Gamma$-$L$ gap energy | 0.20 | | | | | eV |
| $n$ [a] | Refractive index | 4.27 | | | | | |
| $m^*$ [c] | Electron effective mass at $\Gamma$ | 0.036 | | | | | $m_e$ |
| $m_L^{l*}$ [d] | Longitudinal effective mass at $L$ | 1.267 | | | | | $m_e$ |
| $m_L^{t*}$ [d] | Transverse effective mass at $L$ | 0.083 | | | | | $m_e$ |
| $\Gamma_I^i$ [e] | Ionic damping constant | | 6 | 8 | 4 | 12 | $\mathrm{cm}^{-1}$ |
| $\omega_{\mathrm{TO},i}$ [f] | $A_1$(TO) frequency | | 247.7 | 223.4 | 229.5 | 193.6 | $\mathrm{cm}^{-1}$ |
| $\Omega_{P,i}^{0\ 2}$ [e] | Ionic plasma frequency squared | | 11.798 | 4.239 | 11.233 | 4.584 | $10^3\ \mathrm{cm}^{-2}$ |
| $C_i^0$ [g] | Faust-Henry coefficient | | −0.55 | −0.21 | −0.61 | −0.36 | |
| $\varepsilon_{\infty,i}$ [h] | High-frequency dielectric constant | | 10.9 | 14.4 | 12.2 | 15.7 | |

[a]Reference 10.
[b]Reference 18.
[c]Composition-averaged GaSb (Ref. 36) and $InAs_{0.17}Sb_{0.13}$ (Ref. 37) values (see Ref. 18).
[d]Composition-averaged values of the constituent binaries taken from Refs. 36, 38, and 39.
[e]Line-shape fit to 80 K Raman spectrum of control sample ($N_e=0$).
[f]Estimated from 80 K Raman spectrum of the highest electron-density sample.
[g]Reference 40.
[h]References 41–44.

and energy conservation hold. Thus the SPE regime is defined as the energy-momentum region where

$$\hbar\omega_{\mathrm{spe}} = E(\mathbf{k}+\mathbf{q}) - E(\mathbf{k}). \tag{17}$$

Owing to the narrow band gap in $Ga_{1-x}In_xAs_ySb_{1-y}$, the electron effective mass is quite small. Also, the presence of heavy ions (In, Sb) in the alloy results in the corresponding sublattice modes displaying relatively low frequencies. Consequently, the SPE regime extends into the phonon-mode frequency region, where Landau-damping effects are expected to be important.

To estimate the Landau-damping region we use Eq. (17), where $E(\mathbf{k})$ is given by Eq. (12) and the electron wave vector $\mathbf{k}$ is replaced by a suitably averaged value that is determined according to the following considerations. In a classical picture, Landau damping occurs when the phase velocity of the wave, $v_p=\omega_{\mathrm{SPE}}/q$, is comparable to the rms velocity of the electrons. In the classical limit, the relevant velocity is given by $\langle v^2\rangle^{1/2}$, whereas in the degenerate limit at $T=0$ K this is replaced by the Fermi velocity, $v_F$.[29] For finite temperature, we interpolate between these two limits by averaging $\langle k^2\rangle^{1/2}$ over the energy region $E_F \pm 4k_BT$ of the Fermi-Dirac distribution where empty electron states are available.

Intraband electronic transitions which give rise to Landau damping in the single-particle excitation regime are intrinsically considered in the LM model [see Eq. (8)], whereas no account of the distribution of electrons over the available energy states is made in the Drude or HD models. Although single-particle excitations are absent in the HD model, the hydrodynamic pressure-gradient effects introduce a pole on the real axis of the HD susceptibility at $\omega=q\langle v^2\rangle^{1/2}$ that displaces the zeros of the dielectric function. The associated peak in the imaginary part of the susceptibiliy implies a strong damping around the singularity. The HD model, however, cannot be expected to be reliable close to the singularity. In that region only the LM model can account for Landau damping in the electron gas.

## IV. RESULTS AND DISCUSSION

### A. Raman modes in undoped GaInAsSb

In order to test the dielectric alloy model discussed in the preceding section and to obtain an experimental determination of the LO mode frequencies of the alloy, we performed Raman-scattering measurements on an undoped $Ga_{0.85}In_{0.15}As_{0.13}Sb_{0.87}$ control sample. The Raman spectrum of the control sample at 80 K is shown in Fig. 1. The spectrum is dominated by strong peaks at 250.9 and 235.6 $\mathrm{cm}^{-1}$. We assign these peaks to the GaAs-like and InAs-like LO modes of the alloy. A weak peak is also detected at 195.0 $\mathrm{cm}^{-1}$, which is assigned to the InSb-like LO mode. Also, a shoulder on the low-frequency side of the InAs-like LO peak can be observed at 224.3 $\mathrm{cm}^{-1}$ and this can be assigned to the GaSb-like LO mode. As an aid to accurately determine the LO mode frequencies, the second derivative of the spectrum[45] was numerically evaluated (thin line in Fig. 1).

The dielectric model of Sec. III for $N_e=0$ was used to simulate the Raman spectrum and to extract the relevant parameters (phonon frequencies and dampings of the alloy modes). The line shape calculated with the parameters listed in Table I is plotted with a dotted line in Fig. 1. The intensity

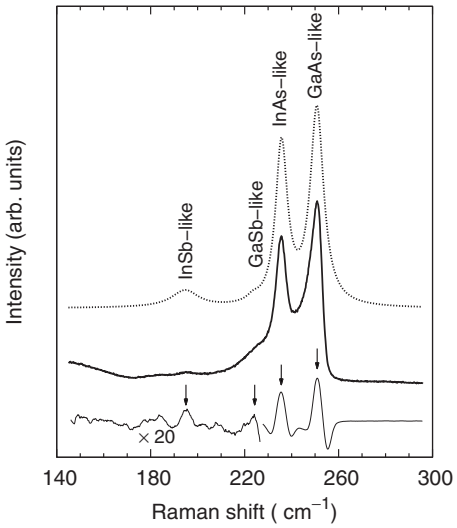


FIG. 1. Raman spectrum of an undoped $Ga_{0.85}In_{0.15}As_{0.13}Sb_{0.87}$ control sample at 80 K (solid line). The lower trace (thin solid line) corresponds to the negative second derivative of the spectrum. The arrows mark the frequencies of the alloy LO modes. The dotted line shows the line shape calculated using the theoretical model of Sec. III for $N_e=0$.

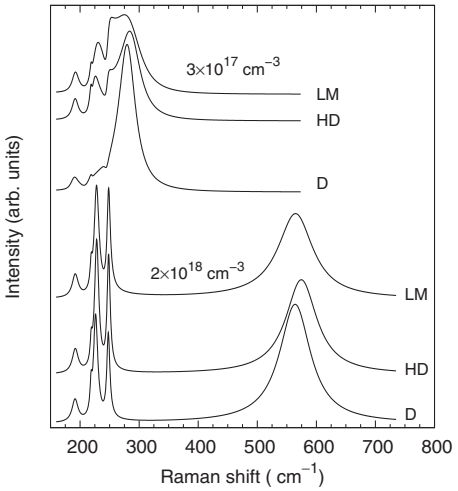


FIG. 2. Raman line shapes calculated for $n$-type $Ga_{0.85}In_{0.15}As_{0.13}Sb_{0.87}$ with $N_e=3\times10^{17}$ cm$^{-3}$ and $N_e=2\times10^{18}$ cm$^{-3}$ ($T=80$ K) using the Drude (D), hydrodynamic (HD), and Lindhard-Mermin (LM) models.

of the InAs-like LO mode is remarkably high, considering that the In-As bond has the lowest relative concentration in the alloy. In contrast, the GaSb-like LO mode is barely visible in spite of the fact that the Ga-Sb bond has the highest relative concentration. This unexpected Raman intensity distribution can be explained by the coupling of the respective sublattice oscillators via the macroscopic electric field of the LO modes, which causes oscillator strength transfer from the majority lower frequency GaSb-like oscillator to the higher frequency InAs-like one. A similar coupling effect was reported in the InGaAs alloy between InAs-like and GaAs-like modes.[17,46,47] In the case of $Ga_xIn_{1-x}As_ySb_{1-y}$, the dominance of the InAs-like oscillator intensity has led in previous studies to consider this alloy within a three-mode behavior framework and to assign the Raman peak observed at about 230 cm$^{-1}$ to (GaSb+InAs)-like mixture modes.[7,8]

On the other hand, the intensity of the InSb-like LO mode is very weak in the Raman spectra. In fact, this mode was not detected in previous Raman-scattering studies.[7,8] A larger value of ionic damping (see Table I) had to be used for the InSb sublattice in the model to simulate the low intensity of the InSb-like LO mode. Even with this high ionic damping, the calculated intensity is higher than the observed Raman peak. We attribute the low intensity of the InSb-like LO mode in the Raman spectra to a poorer quality of the InSb sublattice, which may be affected by Sb segregation problems. In our samples we did not, however, observe the Raman peak at $\approx$160 cm$^{-1}$ that was previously associated with metallic Sb clusters.[9,48]

### B. LOPCM line-shape model analysis

In Fig. 2 we compare the line shapes calculated for $n$-$Ga_{0.85}In_{0.15}As_{0.13}Sb_{0.87}$ at $T=80$ K for electron densities in the lower and upper ends of the range studied using the different models discussed in Sec. III. As can be seen in Fig. 2, whereas the line shapes are very similar at high electron densities, the predictions of the various models differ substantially at low electron densities. At high electron densities the $L^+$ mode is almost entirely plasmonlike and thus very sensitive to charge-density variations. This can be exploited to probe the electron density in the layers by means of contactless optical measurements.[18] We note that, for the range of electron densities studied, the Drude model with the wave-vector correction to the plasma frequency [Eq. (10)] yields nearly the same $L^+$ frequency as the LM model, whereas the HD model tends to give a higher $L^+$ frequency. In the low electron-density range the Drude model predicts an intense undamped $L^+$ mode which dominates the spectrum, whereas the $L^+$ mode is substantially damped according to the LM calculations. The HD model also yields a somewhat damped $L^+$ mode but the intermediate-frequency coupled modes are shifted to lower frequencies. In order to investigate the LOPCM behavior predicted by the various models, we have determined the frequency of the LOPCM line-shape peaks calculated for nominal low values of the damping parameters ($\Gamma_l^i=2$ cm$^{-1}$ and $\Gamma_e=10$ cm$^{-1}$). In Fig. 3 we plot the $n$-$Ga_{0.85}In_{0.15}As_{0.13}Sb_{0.87}$ LOPCM frequency dependence on electron density thus obtained from the Drude (dashed line) and HD (solid line) models at 80 K. The Drude model results follow the generalization of the classical coupled-mode behavior in alloys reported for instance in AlGaAs.[15] Away from the phonon-mode frequencies, plasmonlike modes $L^-$ and $L^+$ exist whose frequencies increase as $\sim N_e^{1/2}$. In the phonon-mode frequency range, three additional intermediate coupled modes appear and their frequencies continuously evolve from the LO frequency of a given sublattice to the higher-lying TO frequency of the next sublattice. The HD model gives basically the same mode behavior, although the proximity of the pole at $q\langle v^2\rangle^{1/2}$ displaces the transition region from LO-phononlike character (low $N_e$) to TO-phononlike character (high $N_e$) of the intermediate

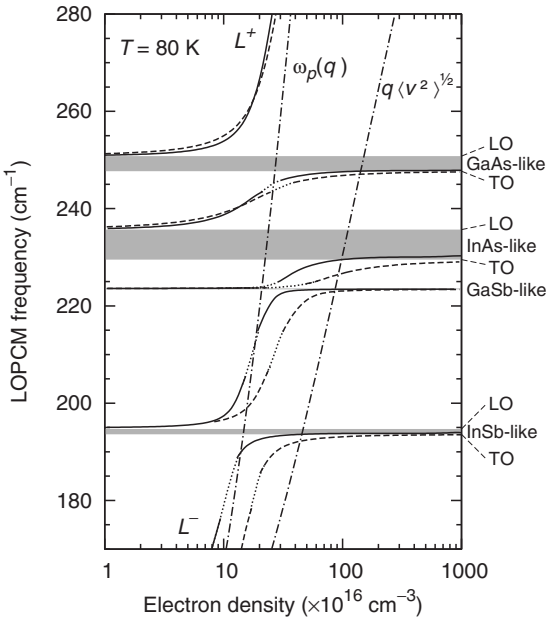


FIG. 3. Carrier density dependence of the LOPCM frequencies of $n$-$Ga_{0.85}In_{0.15}As_{0.13}Sb_{0.87}$ at 80 K calculated using the Drude model (dashed lines) and the hydrodynamical model (solid lines) for $\Gamma_I^i=2$ cm$^{-1}$ and $\Gamma_e=10$ cm$^{-1}$. The shaded areas indicate the reststrahlen region between the TO and LO frequencies of the quaternary alloy. The dotted segments of the curves correspond to regions where the modes are weak and/or ill defined because of interaction terms in the scattering cross section. The pole on the real axis of the hydrodynamic susceptibility $q\langle v^2\rangle^{1/2}$ and the wave-vector-dependent plasma frequency $\omega_p(q)$ are plotted as dashed-dotted lines.

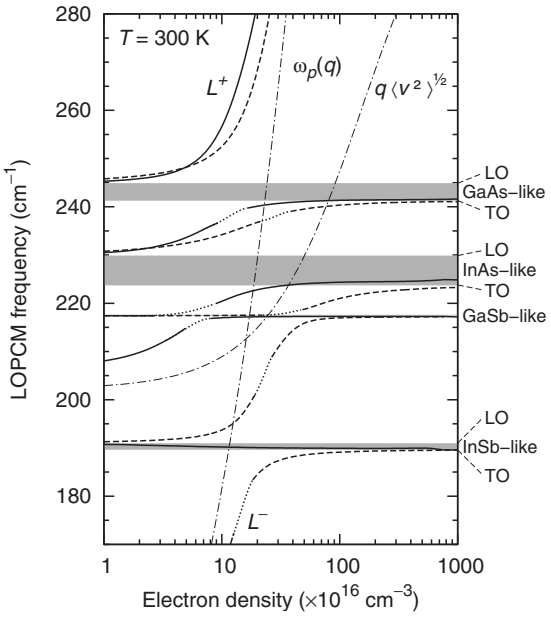


FIG. 4. As in Fig. 3 but for $T=300$ K.

modes toward lower electron densities. In this region, the intermediate modes recover plasmonlike character and their frequencies increase with $N_e$. Similarly, the HD model predicts the evolution of the $L^-$ mode character from plasmonlike to phononlike to occur at lower electron densities. This picture changes at room temperature since then the mean-square velocity of the electrons is higher and the InSb-like phonon frequency lies below the pole in the HD susceptibility. This is illustrated in Fig. 4, where the $n$-$Ga_{0.85}In_{0.15}As_{0.13}Sb_{0.87}$ coupled-mode behavior given by the Drude and LM models is plotted for $T=300$ K. Whereas the Drude model predicts essentially the same coupled-mode behavior at both temperatures, significant differences can be found in the coupled-mode behavior predicted by the HD model. Thus, at 300 K the lowest-frequency intermediate coupled mode is strongly affected by the proximity of the singularity in the HD susceptibility and the $L^-$ mode is replaced by a phononlike mode within the InSb phonon-mode region whose frequency decreases from the LO to the TO InSb-like frequencies. Note that although the behavior of this mode mimics that of an overdamped coupled mode,[35,49] the imaginary HD susceptibility is peaked around the pole and therefore this behavior cannot be attributed to strong damping. As already discussed, the HD model is not expected to give reliable results for $\omega \lesssim q\langle v^2\rangle^{1/2}$.

The mode behavior predicted for the intermediate coupled modes by the LM model is radically different. In Fig. 5 we plot the coupled-mode frequencies obtained from the LM model for $T=300$ K. The $L^+$ mode can be unambiguously identified in the simulated line shapes only for $N_e \gtrsim 2 \times 10^{17}$ cm$^{-3}$. Moreover, since the SPE region (light shaded area below the dashed curve) embraces the phonon-mode frequencies, heavy Landau damping of the intermediate modes occurs in this region, which results in mode frequencies evolving from the LO to the TO frequencies of each sublattice as electron density increases. This behavior can be understood as follows, in analogy with the case of overdamped modes.[35] In the GaAs-like phonon region, at low electron densities the electron plasma cannot screen effectively the LO field and the coupled mode occurs nearly at the LO frequency. As the electron density increases, the LOPCM

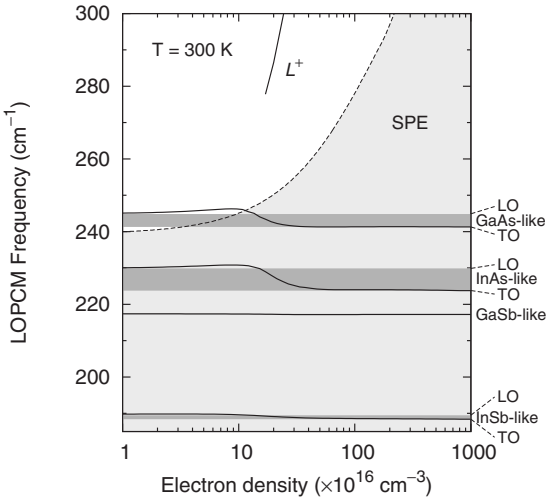


FIG. 5. Coupled-mode behavior calculated using the LM model for $\Gamma_I^i=2$ cm$^{-1}$ and $\Gamma_e=10$ cm$^{-1}$ and $T=300$ K. The light shaded region indicates the extent of the single-particle excitation region. Dark shaded areas correspond to the restrahlen region between the TO and LO mode frequencies.

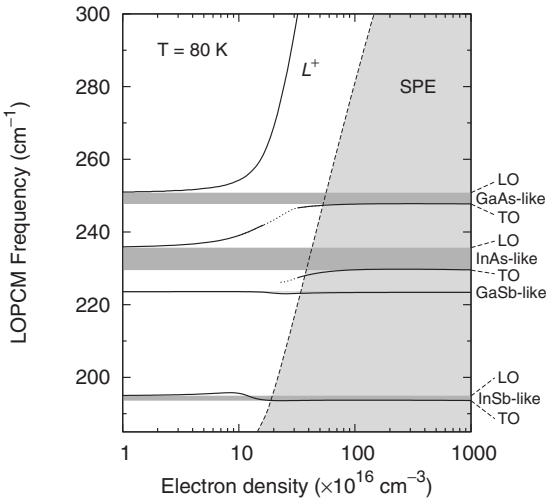


FIG. 6. As in Fig. 5 but for $T=80$ K.

frequency tends to increase. However, as it enters the SPE region a substantial energy transfer takes place from the LOPCM to the electrons that preclude further increment of the LOPCM frequency. While unable to sustain plasmonlike modes, the electron gas becomes more effective in screening the LO field as the electron density increases and the LOPCM frequency falls below that of the LO mode. Only at $N_e \gtrsim 2\times 10^{17}$ cm$^{-3}$, where the plasmon energy lies above the SPE region, a plasmonlike $L^+$ mode develops. For high electron density, all intermediate LOPCMs approach the TO frequencies of the corresponding sublattices. In this regime the plasmonlike modes in the intermediate LOPCM region are suppressed by Landau damping but the high density of mobile electrons yields nearly perfect screening of the LO fields. This gives rise to intermediate LOPCM modes at the TO frequency analogous to the $L^-$ modes reported in highly degenerate, high-mobility III-V binary semiconductors.[11,12] It should be noted that, unlike the case of heavily damped electron plasmas as those occurring for instance in dilute GaAsN,[49] the Landau-damped phononlike intermediate LOPCM modes of the quaternary alloy actually approach asymptotically the TO-phonon frequencies.

The effect of Landau damping on the coupled-mode behavior is clearly demonstrated if we compare the electron-density dependence of the modes at 300 and 80 K. The latter is shown in Fig. 6, where it can be seen that in that case the intermediate coupled modes lie partly outside the SPE region. Then, at 80 K the $L^+$ mode evolves continuously from the GaAs-like LO frequency and the highest intermediate mode frequency also increases with $N_e$ from the InAs-like LO to the GaAs-like TO frequency. This is precisely the behavior predicted by the classical models where Landau damping is not considered (see Fig. 3). Interaction terms between the upper two intermediate modes in their plasmonlike transition region makes these modes ill defined for electron densities between 1.5 and $3\times 10^{17}$ cm$^{-3}$ (dotted lines in Fig. 6). In contrast with the Drude and HD model results, the lower two intermediate modes derived from the LM model display a dominant phononlike character which is more marked as they approach the SPE region. Although the lowest intermediate mode initially increases in frequency, it falls back to the InSb-like TO frequency as it enters the SPE region. In the high electron-density limit all intermediate modes are Landau damped and, as discussed above, their frequencies approach the TO-phonon frequencies.

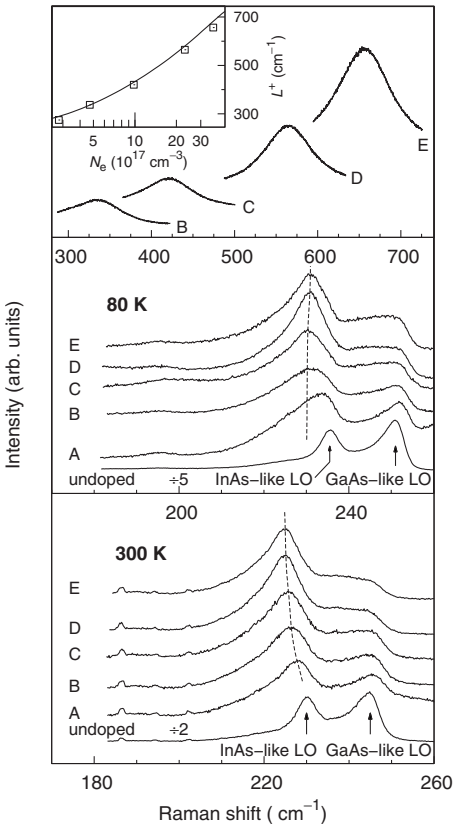


FIG. 7. Raman spectra of $n$-type doped $Ga_{0.85}In_{0.15}As_{0.13}Sb_{0.87}$ samples at 80 and 300 K in the phonon-mode frequency region. The spectrum of an undoped sample is also shown for comparison purposes. In the top panel we display the $L^+$ frequency region for 80 K and the $L^+$ frequency dependence on $N_e$ as obtained from a LM model calculation (inset). The free-electron densities as determined from Hall effect are (A) $2.8\times 10^{17}$ cm$^{-3}$, (B) $4.8\times 10^{17}$ cm$^{-3}$, (C) $9.7\times 10^{17}$ cm$^{-3}$, (D) $2.1\times 10^{18}$ cm$^{-3}$, and (E) $3.7\times 10^{18}$ cm$^{-3}$. The dashed lines are guides to the eye for the frequency dependence on $N_e$ of the InAs-like coupled mode.

### C. Raman spectra of doped $n$-GaInAsSb

In Fig. 7 we display the Raman spectra of five $n$-$Ga_{0.85}In_{0.15}As_{0.13}Sb_{0.87}$ layers, with free-electron densities (A) $2.8\times 10^{17}$, (B) $4.8\times 10^{17}$, (C) $9.7\times 10^{17}$, (D) $2.1\times 10^{18}$, and (E) $3.7\times 10^{18}$ cm$^{-3}$, as determined by Hall measurements. The spectrum of the undoped $Ga_{0.85}In_{0.15}As_{0.13}Sb_{0.87}$ sample is also shown for comparison purposes. In the high-frequency region, all of the doped samples display a clear $L^+$ peak whose frequency shifts by ~400 cm$^{-1}$ over the free-charge density range studied. The Raman spectra of samples B to E in this frequency region are shown in the upper panel of Fig. 7. For sample A the $L^+$ mode lies closer to the GaAs-like phonon region, outside of the frequency range displayed. A full spectrum of sample A can be seen in Fig. 8 (lower panel). The $L^+$ frequency is very sensitive to the free-electron

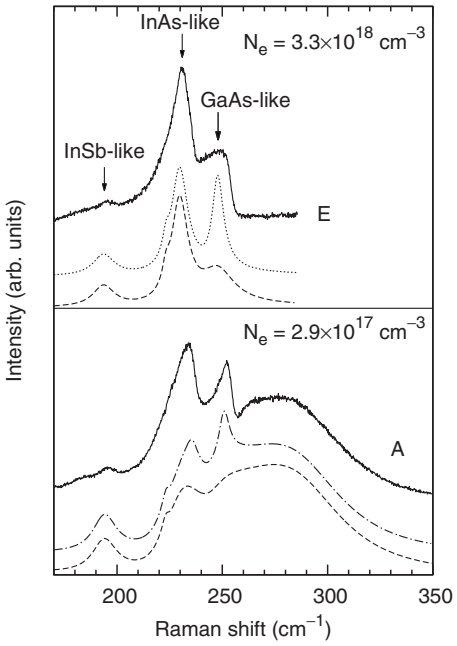


FIG. 8. 80 K Raman spectra of LOPCMs (solid line) in the phonon-frequency region for the lowest (lower panel, sample A) and highest (upper panel, sample E) electron densities studied in this work, compared with line-shape simulations. The dashed lines were calculated using a $\Gamma_l^{(i=1)}$ (GaAs-like) value three times higher than the one listed in Table I. The dotted line in the upper panel was obtained with the $\Gamma_l^{(i=1)}$ given in Table I. In the lower panel, a contribution of the unscreened LO modes from the surface depletion region has been added, with a relative weight of 0.1. The $N_e$ values given in the figure labels were obtained from line-shape fits to the $L^+$ mode.

density in the $n$-$Ga_{0.85}In_{0.15}As_{0.13}Sb_{0.87}$ layers and, as can be seen in the inset, the $L^+$ frequency dependence on $N_e$ is well described by the model calculations. This makes Raman scattering a suitable technique for the determination of electron concentration in $n$-type GaInAsSb.[18] In the phonon-mode region, the doped samples exhibit a significant intensity reduction as well as a shift and a broadening of the peaks relative to the undoped control sample. This is most apparent for the peak in the InAs-like phonon-frequency region, which becomes the dominant peak in doped samples and is located $\sim 4$ $cm^{-1}$ below the InAs-like LO frequency of the undoped sample. For the room-temperature spectra (lower panel of Fig. 7), this peak shifts to lower frequencies as the electron density increases (dotted line), in agreement with the mode dispersion calculated by using the LM model (see Fig. 5). This behavior reflects the overdamped nature of these modes over the whole electron-density range studied. In contrast, in the spectra taken at 80 K (Fig. 7, middle panel) the InAs-like LO peak is observed nearly at the same frequency in the higher electron-density samples (C–E), whereas this peak broadens and takes an asymmetric line shape in the lower electron-density samples (A and B). The model calculations shown in Fig. 6 predict that for $N_e \gtrsim 10^{18}$ $cm^{-3}$ this mode should be well within the Landau-damping region and thus its frequency asymptotically close to the InAs-like TO frequency, as observed for samples C–E. On the other hand, for lower densities this coupled mode should slightly decrease in frequency as it emerges from the Landau-damping boundary. However, as the electron density decreases the depletion layer width increases and the contribution of the uncoupled LO modes from the depletion region becomes more prominent. This explains the observed broadening of this coupled-mode peak and its seeming tendency to the InAs-like LO frequency in samples A and B.

Another striking feature of the coupled-mode Raman spectra of $Ga_{1-x}In_xAs_ySb_{1-y}$ in the phonon-frequency range is the low intensity of the coupled mode occurring in the GaAs-like phonon region. While the model calculations indicate that the coupled-mode intensities in the InAs-like and at GaAs-like phonon-frequency regions should be of similar intensity (see Fig. 2), the latter is barely visible in the Raman spectra. Note that the peak at the GaAs-like LO frequency that can be seen in the spectra of samples A and B is due to the uncoupled LO mode of the surface depletion layer. For samples with higher electron density, where the width of the depletion layer is reduced, only a broad band is observed in this region. The low intensity of the GaAs-like mode cannot be explained in terms of oscillator strength transfer since this was reported to occur in InGaAs from the lower frequency InAs-like modes to the higher frequency GaAs-like modes.[46,47] Then, the low intensity of the GaAs-like coupled mode suggests that this mode is more strongly damped than the InAs-like coupled mode. Given that this coupled mode is associated with the GaAs sublattice, we speculate that the extra damping arises from scattering with the Te impurities, which on account of the similar covalent radii of Ga, As, and Te, may occupy preferentially substitutional As sites in the GaAs sublattice.

In Fig. 8 we compare the Raman spectra in the phonon-frequency region (solid lines) with theoretical line-shape calculations (dotted and dashed lines) for the samples with the highest and lowest electron densities studied (samples E and A, respectively). In the case of sample E, the line shape calculated with the parameters listed in Table I (dotted line) markedly differs in the GaAs-like frequency range from the measured Raman spectrum. However, a much better agreement is obtained if we increase the ionic damping parameter for the GaAs sublattice. The dashed line shown in Fig. 8 was obtained using a GaAs-like $\Gamma_l$ value three times higher than that derived from the Raman spectrum of the undoped sample. This result supports our interpretation that the low intensity of the GaAs-like mode is related to extra damping in the GaAs sublattice. The InSb-like mode is also weaker in the Raman spectra as compared to the calculated line shape. As already discussed for the undoped sample, this is most likely due to a poorer quality of the InSb sublattice associated with Sb segregation problems.

For the sample with the lowest electron density (Fig. 8, lower panel), the calculated line shape also differs from the experimental Raman spectra. As discussed above, this is due to the contribution of the uncoupled LO modes from the surface depletion region. We can reproduce the overall features observed in the Raman spectrum if we add to the calculated LOPCM line shape the spectrum of the undoped sample suitably scaled by a weight factor. This illustrated by

the dotted line in the lower panel of Fig. 8, which was calculated using a relative weight $R=0.1$ for the undoped spectrum as obtained by adjusting the intensity of the GaAs-like mode. From the relation

$$R = \frac{1-\exp(-2\alpha z_0)}{\exp(-2\alpha z_0)}, \tag{18}$$

where $\alpha = 8.35 \times 10^4$ cm$^{-1}$ is the absorption coefficient of the alloy at the 780 nm wavelength, we obtain a depletion depth for this sample of $z_0 \sim 5.7$ nm. Using the simple band-bending model proposed by Pinczuk *et al.*,[50] we estimate from this value a band bending $V_B \sim 30$ meV at the $Ga_{0.85}In_{0.15}As_{0.13}Sb_{0.87}$/air interface. Assuming the same $V_B$ value, we find a depletion depth $z_0 \sim 1$ nm for the sample with the highest electron density, which corresponds to a relative weight of the uncoupled LO in the spectrum of $R \approx 0.017$. Therefore, in that sample the Raman spectrum is virtually unaffected by the presence of the depletion layer and it actually reflects the LOPCMs occurring in the phonon-frequency region.

Additional Raman measurements were carried out at room temperature. No noticeable broadening was observed for the LOPCMs in the phonon-frequency region relative to the 80 K spectra. This reflects the strong phononlike character of these modes and the predominant role of alloy disorder in the determination of their lifetime. A downward shift of about 6 cm$^{-1}$ is observed for the dominant InAs-like peak, which follows the temperature dependence of the InAs-like TO mode. The $L^+$ peak exhibits however much larger shifts, particularly in the samples with higher carrier density. In Fig. 9 we compare the $L^+$ spectra of samples C–E obtained at room temperature (lower panel) and at 80 K (upper panel). For sample E we find an $L^+$ temperature shift of $\approx 33$ cm$^{-1}$ while for sample C the shift is $\approx 14$ cm$^{-1}$. We attribute the temperature dependence of the $L^+$ frequency to the $L$ minima thermal filling effects, which are more important for the samples with higher $N_e$. According to Eq. (14), the electron population of the $L$ valleys at room temperature is estimated at $8 \times 10^{15}$, $1.7 \times 10^{16}$, $6.2 \times 10^{16}$, $3.5 \times 10^{17}$, and $1.1 \times 10^{18}$ cm$^{-3}$ for samples A to E, respectively, whereas it is negligible at 80 K.

Given that the electron mobility in the $L$ valleys is much lower than that at the $\Gamma$ valley, populating the $L$ minima effectively reduces the density of the high-mobility electron gas in the $\Gamma$ valley and this results in a lower frequency of the plasmonlike coupled mode. The LOPCM line-shape model has been fitted to the $L^+$ Raman spectra both at 300 and 80 K. The calculated line shapes and the fitted $N_e$ values are shown in Fig. 9. Given the uncertainty in the model parameters, the $N_e$ values derived from the 300 and 80 K fits are fairly consistent. If the population of the $L$ minima is neglected in the model, i.e., if we assume that all electrons are in the $\Gamma$ valley, we obtain for $T=300$ K the line shapes plotted as dotted lines in Fig. 9. We can see that neglecting the population of the $L$ valley results in an upward $L^+$ frequency shift which increases with $N_e$. This would lead to a substantial underestimation of the electron density in samples with high $N_e$. In contrast, the line shapes calculated at 80 K are virtually unchanged, which indicates that the thermal population of the $L$ minima is negligible in this case.

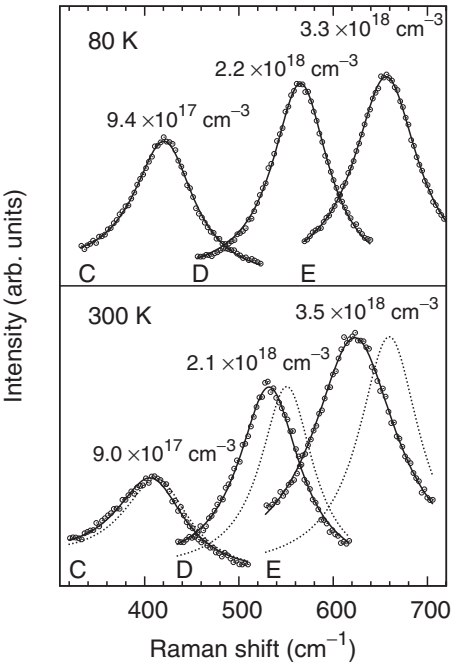


FIG. 9. Raman spectra (circles) of the $L^+$ coupled mode of the three samples with higher electron density (C–E) taken at room temperature (lower panel) and at 80 K (upper panel). The line-shape model fits to the spectra obtained for the $N_e$ values shown in the figure are plotted as solid lines. The dotted lines in the lower panel represent the calculated $L^+$ line shapes for the same $N_e$ values when the filling of the secondary $L$ minima is neglected.

## V. SUMMARY AND CONCLUSIONS

The phonon modes of the $Ga_{1-x}In_xAs_ySb_{1-y}$ alloy and their coupling with plasma excitations have been studied by means of Raman scattering. A generalization of the dielectric Raman line-shape model to the quaternary alloy has been described. Our experimental results on a sample with $x=0.15$ and $y=0.13$ are consistent with a four-mode behavior of the alloy, albeit with a significant oscillator strength transfer from the GaSb-like to the InAs-like modes and a weak oscillator strength of the InSb-like mode, probably related to sublattice disorder. In this context, Drude type, hydrodynamical, and LM expressions for the free-electron susceptibility have been employed and their influence on the calculated line shape has been analyzed. While the plasmonlike $L^+$ mode is adequately described by any of the models studied, substantial differences between the classical models and the LM model arise for the lower frequency LOPCMs occurring in the phonon-frequency region. These differences are traced to the Landau-damping effects on these modes, which are only taken into account in the LM model. Most of the lower frequency LOPCMs are thus overdamped modes with frequencies close to the TO frequencies of the sublattices. In the $n$-type layers, the dominant Raman peak corresponds to the

InAs-like LOPCM, whereas the GaAs-like LOPCM appears to be more strongly damped.

Because of the combination of small electron effective-mass and low phonon frequencies of the $Ga_{0.85}In_{0.15}As_{0.13}Sb_{0.87}$ alloy, the lower LOPCM modes lie within the Landau-damping region depending on the temperature and the electron density of the samples. The change in the Landau-damping regime of the dominant InAs-like LOPCM mode that takes place from room temperature to 80 K gives rise to a different electron-density dependence of the frequency of this mode. This is observed in the Raman spectra of our set of samples obtained at 300 and 80 K.

The population of the $L$ minima is increasingly important in samples with higher electron density at room temperature, whereas it is negligible at 80 K. The thermal filling of the $L$ minima explains the substantial downward shifts of the $L^+$ coupled mode observed in the room-temperature Raman spectra relative to the 80 K spectra.

## ACKNOWLEDGMENTS

The authors gratefully acknowledge C. Wang (MIT, Lincoln Laboratory) for supplying the $Ga_{0.85}In_{0.15}As_{0.13}Sb_{0.87}$ epilayers studied in this work and D. A. Shiau for assistance in the growth of the epilayers and in the performance of the single magnetic field Hall-effect measurements. This work has been supported by the Spanish Ministry of Science and Innovation under Contract No. MAT2007-63617.

[1] C. A. Wang, H. K. Choi, S. L. Ransom, G. W. Charache, L. R. Danielson, and D. M. DePoy, Appl. Phys. Lett. **75**, 1305 (1999).
[2] G. W. Charache *et al.*, J. Appl. Phys. **85**, 2247 (1999).
[3] C. Caneau, A. K. Srivastava, A. G. Dentai, J. L. Zyskind, and M. A. Pollack, Electron. Lett. **21**, 815 (1985).
[4] C. A. Wang and H. K. Choi, Appl. Phys. Lett. **70**, 802 (1997).
[5] E. Bowers, A. K. Srivastava, C. A. Burrus, J. C. DeWinter, M. A. Pollack, and J. L. Zyskind, Electron. Lett. **22**, 137 (1986).
[6] M. J. Cherng, H. R. Jen, C. A. Larsen, G. B. Stringfellow, H. Lundt, and P. C. Taylor, J. Cryst. Growth **77**, 408 (1986).
[7] D. H. Jaw, Y. Y. Cherng, and G. B. Stringfellow, J. Appl. Phys. **66**, 1965 (1989).
[8] V. Vorlíček, K. D. Moiseev, M. P. Mikhailova, Y. P. Yakovlev, E. Hulicius, and T. Simecek, Cryst. Res. Technol. **37**, 259 (2002).
[9] J. Díaz-Reyes, E. López-Cruz, J. G. Mendoza-Álvarez, and S. Jiménez-Sandoval, J. Appl. Phys. **100**, 123503 (2006).
[10] M. Muñoz, K. Wei, F. H. Pollak, J. L. Freeouf, C. A. Wang, and G. W. Charache, J. Appl. Phys. **87**, 1780 (2000).
[11] *Light Scattering in Solids IV*, Topics in Applied Physics Vol. 54, edited by M. Cardona and G. Güntherodt (Springer-Verlag, Berlin, 1984), and references therein.
[12] L. Artús, R. Cuscó, J. Ibáñez, N. Blanco, and G. González-Díaz, Phys. Rev. B **60**, 5456 (1999).
[13] M. Ramsteiner, J. Wagner, P. Heisienger, K. Köhler, and U. Rössler, J. Appl. Phys. **73**, 5023 (1993).
[14] R. Cuscó, J. Ibáñez, E. Alarcón-Lladó, L. Artús, T. Yamaguchi, and Y. Nanishi, Phys. Rev. B **79**, 155210 (2009).
[15] T. Yuasa, S. Naritsuka, M. Mannoh, K. Shinozaki, K. Yamanaka, Y. Nomura, M. Mihara, and M. Ishii, Phys. Rev. B **33**, 1222 (1986).
[16] J. E. Maslar, J. F. Dorsten, P. W. Bohn, S. Agarwala, I. Adesida, C. Caneau, and R. Bhat, Phys. Rev. B **50**, 17143 (1994).
[17] R. Cuscó, L. Artús, S. Hernández, J. Ibáñez, and M. Hopkinson, Phys. Rev. B **65**, 035210 (2001).
[18] J. E. Maslar, W. S. Hurst, and C. A. Wang, J. Appl. Phys. **106**, 123502 (2009).
[19] N. D. Mermin, Phys. Rev. B **1**, 2362 (1970).
[20] C. A. Wang, J. Cryst. Growth **191**, 631 (1998).
[21] C. A. Wang, H. K. Choi, D. C. Oakley, and G. W. Charache, J. Cryst. Growth **195**, 346 (1998).
[22] P. C. Mathur, N. D. Kataria, and S. Jain, J. Phys. Chem. Solids **39**, 403 (1978).
[23] D. T. Hon and W. L. Faust, Appl. Phys. (Berlin) **1**, 241 (1973).
[24] T. Inoshita, J. Appl. Phys. **56**, 2056 (1984).
[25] R. Fukasawa and S. Perkowitz, Phys. Rev. B **50**, 14119 (1994).
[26] U. Nowak, W. Richter, and G. Sachs, Phys. Status Solidi B **108**, 131 (1981).
[27] V. Vorlíček, I. Gregora, W. Kauschke, J. Menéndez, and M. Cardona, Phys. Rev. B **42**, 5802 (1990).
[28] J. Ibáñez, R. Cuscó, and L. Artús, Phys. Status Solidi B **223**, 715 (2001).
[29] D. H. Jackson, *Classical Electrodynamics* (Wiley, New York, 1975).
[30] U. Rössler, Solid State Commun. **49**, 943 (1984).
[31] E. O. Kane, J. Phys. Chem. Solids **1**, 249 (1957).
[32] R. Cuscó, E. Alarcón-Lladó, J. Ibáñez, T. Yamaguchi, Y. Nanishi, and L. Artús, J. Phys.: Condens. Matter **21**, 415801 (2009).
[33] P. M. Platzman and P. A. Wolff, *Solid State Physics* (Academic Press, New York, 1973), Suppl. 13.
[34] R. Cuscó, J. Ibáñez, and L. Artús, Phys. Rev. B **57**, 12197 (1998).
[35] K. Wan and J. F. Young, Phys. Rev. B **41**, 10772 (1990).
[36] H. Arimoto, N. Miura, R. J. Nicholas, N. J. Mason, and P. J. Walker, Phys. Rev. B **58**, 4560 (1998).
[37] J. M. Aubin and J. C. Woolley, Can. J. Phys. **46**, 1191 (1968).
[38] J. S. Blakemore, J. Appl. Phys. **53**, R123 (1982).
[39] *Handbook Series on Semiconductor Parameters*, edited by M. Levinstein, S. Rumyantsev, and M. Shur (World Scientific, London, 1996), Vol. 1.
[40] C. Flytzanis, Phys. Rev. Lett. **23**, 1336 (1969).
[41] G. A. Samara, Phys. Rev. B **27**, 3494 (1983).
[42] S. Adachi, J. Appl. Phys. **53**, 8775 (1982).
[43] P. S. Dutta, H. L. Bhat, and V. Kumar, J. Appl. Phys. **81**, 5821 (1997).
[44] J. R. Dixon, Jr. and J. K. Furdyna, Solid State Commun. **35**, 195 (1980).
[45] P. G. Etchegoin, M. Cardona, R. Lauck, R. J. H. Clark, J. Serrano, and A. H. Romero, Phys. Status Solidi B **245**, 1125 (2008).
[46] J. Groenen, R. Carles, G. Landa, C. Guerret-Piécourt, C. Fontaine, and M. Gendry, Phys. Rev. B **58**, 10452 (1998).

[47] K. J. Nash, M. S. Sknolnick, and S. J. Bass, Semicond. Sci. Technol. **2**, 329 (1987).
[48] B. Eberle, H. Sontag, and R. Weber, Surf. Sci. **156**, 751 (1985).
[49] J. Ibáñez, R. Cuscó, E. Alarcón-Lladó, L. Artús, A. Patanè, D. Fowler, L. Eaves, K. Uesugi, and I. Suemune, J. Appl. Phys. **103**, 103528 (2008).
[50] A. Pinczuk, A. A. Ballman, R. E. Nahory, M. A. Pollak, and J. M. Worlock, J. Vac. Sci. Technol. **16**, 1168 (1979).